Available online at www.sciencedirect.com
SCIENCE DIRECT®
Journal of Power Sources 128 (2004) 208–217
JOURNAL OF POWER SOURCES
www.elsevier.com/locate/jpowsour

Operational aspects of a large PEFC stack under practical conditions

Paul Rodatz [a,*], Felix Büchi [b], Chris Onder [a], Lino Guzzella [a]

[a] *Measurement and Control Laboratory, Swiss Federal Institute of Technology (ETH), ETH Zentrum ML, Sonneggstrasse 3, CH-8092 Zurich, Switzerland*
[b] *Electrochemistry Laboratory, Paul Scherrer Institute, CH-5232 Villigen PSI, Switzerland*

Received 20 May 2003; received in revised form 12 September 2003; accepted 29 September 2003

Abstract

Measurement results obtained from single-cell experiments give insight of electrochemical processes and allow for their optimization. However, the operator of large fuel cell stacks is confronted by a different set of problems that do not arise in such small scale experiments. Typically in a fuel cell stack the reactants and the cooling medium are fed in parallel to the cells. This can lead to an uneven flow distribution in the flow channels and an uneven cell voltage distribution across the stack. Therefore, a cleverly devised control and monitoring system is required to ensure that no unbalanced strain is put on the stack. This paper investigates some aspects critical to the operation of large fuel cell stacks in automotive applications such as control issues in the supply system, stack failures, and the appropriate countermeasures as well as some procedures to increase the voltage stability.

Keywords: Fuel cells; Proton exchange membrane (PEM); Stacks; Pressure drop modeling; Voltage variations

1. Introduction

For a given set of operating parameters (such as system pressure, temperature, and gas stoichiometry) the fuel cell voltage is essentially determined by the applied current. All polymer electrolyte fuel cells (PEFC) exhibit similar voltage/current relationships, as illustrated in Fig. 1. The semi-exponential behavior at low current densities is due to the activation overpotential of the oxygen reduction. In the intermediate current density region the pseudolinear behavior is caused predominantly by ohmic losses. At high current densities the cell potential decays rapidly due to mass-transport limitations. At zero current the voltage is the highest. Its value is given by the standard potential of the chemical reaction. The value for the hydrogen–oxygen couple is 1.23 V at standard conditions. However, under practical conditions the open-circuit potential (voltage at zero current) will settle at values slightly below 1 V. This deviation can be explained if the open-circuit potential is considered to be a mixed potential due to the simultaneous occurrence of the two-electron and four-electron oxygen reduction reactions. Impurity oxidation can also contribute to the reduction of the observed open-circuit potential (for more details see [1,2]).

To achieve a high power density (W/kg) of the fuel cell stack, it should be operated at high current densities. However, the current cannot be increased at will, as the power output will reach a maximum due to the falling voltage. After this maximum the power output will decrease with increasing current density. The maximum power density of a fuel cell stack is highly dependent on the operating parameters.

With increasing current density the following aspects have to be considered:

- The fuel cell efficiency decreases along with the decreasing fuel cell voltage.
- The amount of heat which has to be removed from the system increases superproportionally.
- The supply of the reactant gases is proportional to the current.
- The uniformity in cell voltage levels decreases.

Therefore, under practical conditions the fuel cell is often not operated up to the maximum power output. The maximum current density which is applied to the fuel cell system is thus case sensitive and has to be considered under the aspects listed above. The chosen value depends on the setup of the fuel cell system. For well optimized system the value may be as high as 1 A/cm^2.

In this paper, several aspects are discussed, which need to be considered when a fuel cell stack is operated under practical conditions, e.g. in an automotive application. To gain

* Corresponding author. Tel.: +41-1-6325926; fax: +41-1-6321139.
E-mail address: rodatz@imrt.mavt.ethz.ch (P. Rodatz).

0378-7753/$ – see front matter © 2003 Elsevier B.V. All rights reserved.
doi:10.1016/j.jpowsour.2003.09.060

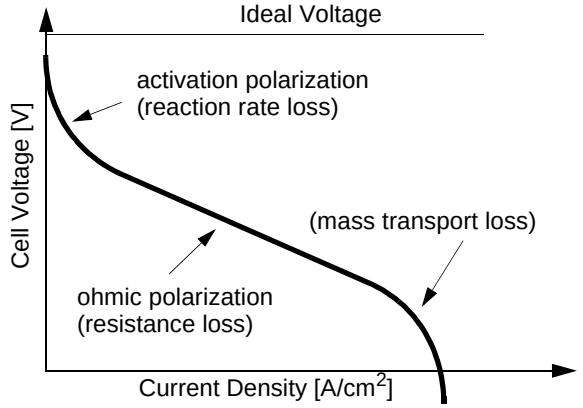

Fig. 1. Typical polarization curve of a H_2/air fuel cell with major loss contributions.

a better insight and a better understanding of the limitations which arise, if a fuel cell is operated under these conditions, a testbench was constructed to reproduce conditions similar to those in an automotive application. An almost identical setup was used in the experimental fuel cell vehicle 'Hy.Power' [3]. In this paper the setup of this testbench is described and some control issues are pointed out. Furthermore, typical causes of failures based on results from the testbench are discussed and procedures are proposed that lead to performance improvements of the fuel cell stack.

2. Experimental setup

The testbench described in this section is closely related to the fuel cell system used in the experimental vehicle Hy.Power, which is a fuel cell powered electric vehicle, assisted by a supercapacitor storage. It was designed and constructed in a joint project by the Paul Scherrer Institute, the Swiss Federal Institute of Technology (ETH) and various industrial partners and has been demonstrated on numerous occasions since its completion in 2002 [3].

The testbench was designed and constructed to be as similar to the vehicle as possible. Many parts used in the testbench are also found in the vehicle. However, the piping in the testbench is longer than in the vehicle in order to avoid any physical constraints caused by components placed in too close vicinity.

2.1. Fuel cell stack

The two main parts of a fuel cell are the bipolar plates and the membrane–electrode-assemblies (MEA). The bipolar plates have to distribute air and hydrogen to the MEA, to comprise the cooling channels, to avoid mixing of the different media, to ensure that none of them leak to the exterior, and to conduct the current between the cells. New bipolar plates have been developed and optimized with regard to volume, weight and manufacturing. More details can be found elsewhere [4]. The MEA is made up from commercially available membranes (Nafion 112, DuPont) and gas diffusion electrodes (ELAT, E-Tek, 0.5 mg Pt/cm^2), while the respective preparation and assembly procedures were newly developed.

The fuel cell stack consists of 100 cells with an active area of 204 cm^2. Under optimal conditions with regard to pressure, humidity, reactants flow, and temperature the electrical output capability of the stack is 6 kW at 0.6 V/cell. The cells are electrically connected in series, while the reactant gases and the cooling liquid are fed in parallel to the cells. Since each cell has 26 flow field channels, a total of 2600 channels have to be supplied.

3. Fuel cell system

The direct hydrogen fuel cell system (see Fig. 2) may be divided into three subsystems according to the fluid it handles:

- air subsystem: supply the process air at the required pressure, flow rate, temperature, and humidity;
- H_2 subsystem: supply hydrogen at the required pressure and flow rate;
- cooling subsystem: guarantee adequate cooling of the fuel cell stack and ensure small temperature gradient across the stack.

3.1. Air supply

The supply of air to the cathode is handled by a twin-screw compressor (Opcon OA1040) and a continuous pressure valve (Bürkert). A supersonic atomizer (Lechler) is used for the humidification of the air stream.

With regard to the air supply of the fuel cell system, four states need to be controlled: mass flow, pressure, inlet temperature, and humidity, but only three actuators are available, namely the compressor, the pressure valve, and the humidification device. By injecting liquid water droplets into the hot air leaving the compressor the air stream is cooled and the humidity is increased. Therefore, the inlet temperature and the humidity are coupled and cannot be controlled independently in this setup. Excessively high inlet temperatures may damage the fuel cell membrane whereas a low humidity results in poor stack efficiency. The amount of injected water is thus used to control the temperature, whereas the humidity is allowed to float.

The control of air mass flow and air pressure was achieved with two independent closed-loop control systems. The mass flow control loop consists of the compressor, a mass flow sensor (TSI 4020), and a simple PI controller. Similarly, the pressure-control loop is made up of the continuous pressure valve (Bürkert), a pressure sensor (Bürkert) and another PI controller. Although mass flow and pressure interact (e.g. an increase in mass flow translates into a higher pressure if the valve position is kept unchanged), experiments have

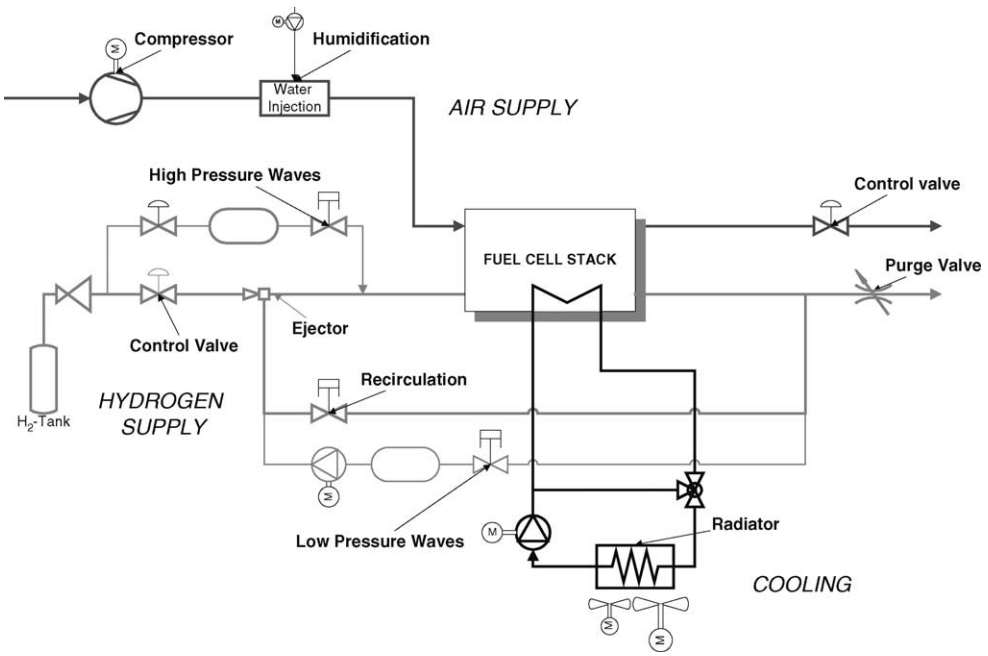

Fig. 2. Diagram of the testbench setup, consisting of air supply, hydrogen supply, and cooling.

proven that the fuel cell acts as a sufficient damping element and that PI controllers provide satisfactory results. Nevertheless, state-based controllers decouple pressure and mass flow more effectively and show a superior behavior with regard to response time and to deviations from the setpoint.

3.2. Hydrogen supply

The hydrogen supply is described in detail elsewhere [5]. In short, hydrogen is stored in a high-pressure tank at up to 200 bar. Using a reduction valve (Gloor) and a control valve (Bürkert) hydrogen is fed to the fuel cell stack. Excess hydrogen is recirculated by means of an ejector (Festo). In addition, pressure waves are used to assist the removal of water droplets in flow channels. These pressure waves are generated in three different ways. First, the fuel cell is periodically supplied (in very short intervals of less than 0.5 s) with hydrogen at pressures higher than the operating pressure. Second, also periodically, hydrogen is sucked from the exit of the fuel cell into a low pressure vessel generating low pressure pulses. The pump used to build up the vacuum in this vessel discharges the hydrogen to the entrance of the fuel cell. Finally, hydrogen is purged to the environment through a valve at the exit of the fuel cell (however, this option is not used under regular operating conditions).

In order to achieve the best performance of the fuel cell stack, mass flow, pressure, inlet temperature, and humidity need to be controlled on the hydrogen side as well. Because of the stringent limitations on space and weight in an automotive application no humidification device was installed in the hydrogen feed. However, since part of the hydrogen is recirculated, dry hydrogen from the tanks is mixed with hydrogen which already passed through the stack and thereby took up water. Experiments have shown that in thin membranes (such as Nafion 112) the water flux due to back-diffusion to the anode can effectively compensate the flux due to the electro-osmotic drag. Hence, the water is more evenly distributed in a thin membrane. Due to the fact that the hydrogen flow is considerably smaller than the air flow, the capacity of hydrogen to carry water is also considerably smaller. Therefore, the lack of a proper humidification device in the hydrogen feed is not considered to be of major concern as the humidification of the air flow is much more important. Furthermore, since the hydrogen expands from high-pressure tanks prior to entering the fuel cell, the danger of excess temperature does not arise. Therefore, in this setup neither temperature nor humidity are controlled on the hydrogen side.

Although the fuel cell stack is fed with a surplus of hydrogen, from a system point of view the fuel supply is a deadend system. As a consequence only one degree of freedom exists to control either mass flow or pressure. A large pressure difference across the membrane between the air and hydrogen side would damage the membrane. Therefore, precautions have to be taken to avoid any large pressure deviations by controlling the hydrogen pressure or the pressure difference across the stack (realized again with a PI controller). The mass flow then adjusts itself according to the pressure drop across the pressure-regulating valve. Under steady-state conditions the hydrogen mass flow into the system equals the hydrogen consumed by the electrochemical reaction. In transient conditions there is lag, which causes a shortage of hydrogen and possibly even a local starvation of the reaction. This phenomenon is avoided by the above-mentioned recirculation of a certain amount of hydrogen, hence by supplying the fuel cell

continually at larger than stoichiometric values. Without this arrangement only very limited dynamics would be achievable.

3.3. Cooling

The configuration of the cooling system is rather straightforward. The liquid cooling loop designed to cool the cells, consists of a continuous-controlled pump and a radiator with two fans of different size (standard automotive parts). The fans are operated independently, although only in an on–off mode. As the cells are fed in parallel, it is difficult to obtain an equal flow through all cells, especially at reduced flows. At low flows insufficient cooling and hot spots in the membrane may occur, as some cells may not be properly fed with cooling liquid. This is avoided by not operating the pump in the region with small flows. Sufficient flows in all cells are thus achieved even at low fuel cell loads, although at the expense of a slightly higher power consumption. Furthermore, the effect of intensive cooling with an accompanying falling stack temperature has to be accepted, although this effect is lessened if the radiator is bypassed. The pump is controlled by a PI controller, whereas binary controllers control the fans.

The control algorithms are centrally managed by a dSpace™ DS1003 Processor Board. Matlab/Simulink™ is used to program the control algorithms. Logical sequences were programmed with the help of the Matlab toolbox Stateflow™. Euler's method was chosen as a solver, with a fixed step size of 5 ms.

The communication between the sensors and the dSpace system, as well as the communication to the actuators are handled by a CAN-Bus. For this purpose the highly flexible WAGO 750 CANopen series is installed, which is a modular I/O system. Modules are available for almost every type of sensor signal or actuator output, and the configuration can be expanded easily by adding additional elements. The load for dissipating the electric power is a Höcherl & Hackl electronic load, type DS5010, capable to sustain loads of up to 100 A or 5 kW.

4. Failures

Since all cells in a stack are electrically connected in series, the reliability of a stack depends on a satisfactory operation of *all* individual cells. The probability of a stack failure is found to increase with the number of cells in a stack [6]. Thus, stacks with a large number of cells call for special precautions. In the following some typical causes of failures are outlined and feasible countermeasures are discussed.

4.1. Undersupply and negative voltage

In order to sustain the chemical reaction, the cells must be supplied with reactant gases at stoichiometric or preferably higher values, as the completely uniform distribution of the reactant gases to the many channels cannot be guaranteed. An even fluid distribution to all these channels is difficult to achieve, since slight deviations in the flow resistance lead to variations of the flow. At high utilization rates these flow discrepancies translate into variations of the cell voltage across the stack. These discrepancies are assumed to result from liquid water droplets forming in the flow channels and thereby interfering with the gas flow, from small geometric deviations in the channel geometry of the plates, from thermal inhomogeneities and from other effects. An undersupply of the cells with reactant gases will lead to a breakdown of the chemical reaction and a rapid loss in voltage. The voltage might even drop to negative values and decomposition of electrochemical components and local heat generation ("hot spots") would damage the cells permanently. Therefore, an undersupply of reactant gases must be avoided under any circumstances. Special care must be taken particularly under dynamic load changes, when the applied current changes very fast compared to the response of the reactants supply system.

If only the stack voltage is monitored the breakdown of a single cell in a large stack is difficult to detect. In a stack of 100 cells, the failure of one cell causes the stack voltage to decrease by only 1 %. Voltage changes in this range may also be attributed to phenomena occurring throughout the stack such as dehydration of the membranes or flooding of the gas diffusion electrodes. These phenomena cause a slight deterioration in every cell. Therefore, the monitoring of only the stack voltage makes it difficult to distinguish the accumulation of slight deteriorations in all cells from the breakdown of a single cell.

A solution to improve matters is the monitoring of every cell voltage or at least of a small group of cells. Groups of no more than five cells seem feasible, since the failure of a single cell will lead to a drop of at least 20% in the group voltage, which can be identified. However, with single-cell monitoring the wiring increases dramatically. Furthermore, reliable and cost efficient electronics are needed to measure the cell voltages. Once the single-cell monitoring device is installed, appropriate countermeasures must be arranged. The detection of a drop in cell voltage will not give any insight into the cause of the failure. The cell might have failed due to the blocking of channels or reaction sites by excess water, due to overheating by temporarily insufficient cooling or due to a mechanical failure of the membrane. A highly sophisticated diagnosis system is required to decide on the appropriate countermeasure. When a cell failure is detected the complete shutdown of the fuel cell system is the most secure action. However, to maintain the operation of the fuel cell other actions might be more appropriate, such as temporary reduction of the load, increase in stoichiometry of the reactant gases (to blow out excess water) or reduction of the cell temperature (to assist the hydration of the membrane).

4.2. Leaks in membrane

Either mechanical stress or hot spots might cause leaks in the membrane that give way to a direct mixing of hydrogen and oxygen within the cell. In the presence of the electrocatalyst, this leads to a thermal combustion of hydrogen and the generation of heat. This causes the leak to grow, making matters worse. The generation of large amounts of heat will also affect neighboring cells, as the rising temperature causes a dehydration of neighboring membranes, resulting in an increase in the membrane resistance and a consequent rise of the heat generation also in the neighboring cells. In the long run, hot spots will also form in the neighboring cells, causing a domino effect. Hot spots are difficult to detect as the effect is locally limited.

4.3. Overheating

Overheating of the fuel cell stack leads to severe dehydration of the membrane, resulting in a larger resistance and a performance loss. Furthermore, overheating might cause permanent damage to the membrane. In practical applications the temperature of the cooling water will only be measured at the entrance and exit of the fuel cell stack. Therefore, local overheating due to a varying distribution of the cooling water across the stack is impossible to detect. Especially at low circulation rates slight deviations in the flow resistance of the cooling channels might lead to an uneven flow distribution across all channels, thus causing local overheating. Consequently, during the construction process special care must be taken to ensure that all pathways have an equal flow resistance. The formation of air pockets can also contribute to local overheating as the flow of the cooling water is interrupted in this area. Hence the fuel cell should be operated at all times with a sufficient minimum cooling flow to avoid local overheating.

4.4. Large differential pressure

A large pressure difference across the membrane between the reactant gases causes mechanical stress on the membrane and may tear it. Holes in the membrane result in the direct mixing of hydrogen and oxygen and the production of heat through catalytic combustion. The consequence of leaks in the membrane has already been discussed in Section 4.2. To avoid large pressure differences, controllers that react swiftly to pressure changes ($\tau < 50$ ms) are required. Countermeasures must be taken against fast pressure changes due to valve malfunctioning, bursts in the piping or controller over-/undershoots. As a first measure, pressure relief valves should be installed. Further, the pressure-control valve should be of normally open type to allow the gases to escape if the power supply fails. Additionally, a device is required which can react to large differential pressures. This may be accomplished either by a control algorithm using pressure sensors and valves or better by a purely mechanical device. The main advantage of a mechanical device is that it is not impaired by controller malfunctioning, interrupts in the power supply, or loose contacts in the wiring.

5. Results and discussion

5.1. Voltage distribution in stack

The stack voltage divided by the number of cells in the stack gives the mean cell voltage. As Fig. 3 shows (at three different current levels), the actual cell voltages differs from this mean voltage. The mean voltage and the standard deviation are shown as a function of the current density in Fig. 4. In the region of low current densities the deviations are small, whereas at high current densities they may amount

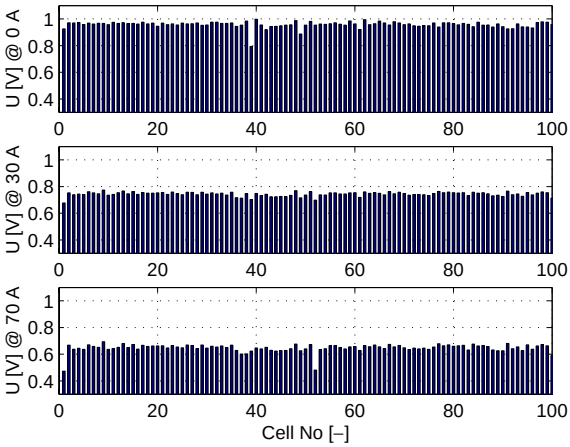

Fig. 3. Measured variation in single-cell voltage of a 100-cell stack at various current levels (active area 204 cm^2). Cell temperature, 60 °C; air dew point, 45 °C; air stoichiometry, 2.2; air/hydrogen pressure, 2/2.2 bar_{abs}.

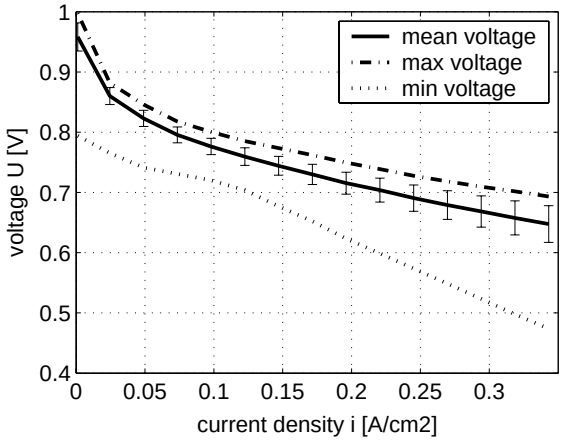

Fig. 4. Measured mean voltage of 100-cell stack with standard deviation. Also shown are the minimum and maximum voltage levels. Stack was operated at 30 A (0.15 A/cm^2) for 30 min prior to recording. Cell temperature, 60 °C; air dew point, 45 °C; air stoichiometry, 2.2; air/hydrogen pressure, 2/2.2 bar_{abs}.

to 5% or more of the mean voltage. Fig. 4 also shows the maximum and minimum voltages, whereby in this particular stack especially the minimum voltage deviates substantially from the mean.

Variations in the cell voltages are the cumulative result of at least four sets of factors:

- uneven flow distribution of the reactant gases;
- non-uniform temperature field in the stack;
- different states in the ageing process;
- defects or tolerance of fabrication in particular cells.

The flow distribution is strongly coupled to the flow resistance in the channels and the cells. The pressure loss in piping systems, where the gravitational head may be neglected, is typically calculated as follows:

$$\Delta p = \left(f \frac{l}{d} \right) \rho \frac{v^2}{2} + \sum K \rho \frac{v^2}{2} \tag{1}$$

Here f represents the friction factor, l the channel length, d the hydraulic diameter, ρ the density, v the flow velocity and K is the hydraulic resistance.

Using

$$v = \frac{\dot{V}}{A} = \frac{\dot{V}}{d^2(\pi/4)}$$

where $\dot{V}$ is the flow rate and A the channel cross-section and rewriting Eq. (1) yields:

$$\dot{V} = \sqrt{\frac{\Delta p}{R_\mathrm{k}}} \tag{2}$$

with

$$R_\mathrm{k} = \frac{8\rho}{\pi^2} \left(f \frac{1}{d} + \sum K \right) \frac{1}{d^4} \tag{3}$$

The index k relates to one flow channel. Since all flow channels are fed in parallel, the pressure loss across all cells is the same. Therefore, the flow in each channel will vary with the resistance R_k. The flow resistance is primarily influenced by restrictions in the cross-section of the flow channels. These may be caused by variations in the flow channel depth and width due to fabrication tolerances, the intrusion of the gas diffusion electrode, or an accumulation of water droplets. The pressure drop across the stack is discussed in more detail in the next section.

The second set of factors causing variations in the cell voltages relates to the temperature distribution inside the fuel cell, which has an important effect on nearly all transport phenomena [7]. A non-uniform temperature distribution may arise from varying flow resistance in the flow channel of the cooling media, air pockets in the channel, or variations in the membrane resistance and a resulting variation in local heat generation.

The third set of factors deals with differences in the ageing process. It has been shown in [8] that longtime exposure to excess water facilitates the poisoning of the active layer of the gas diffusion electrode, thereby accelerating the ageing process. Especially the cells closest to the inlet are at risk of being exposed to excess water, as any water which might have condensed in the piping will most probably pass through the flow channels of these cells.

The final set of factors relates to faults in the material or defects which occurred during the assembly of the stack. These may include weak points in the membrane, flaws in the bipolar plates, uneven distribution of the catalyst on the gas diffusion electrode, or insufficient contact between gas diffusion electrode and membrane. All these factors lead to additional losses, thereby decreasing the voltage.

In a fuel cell stack the cell with the poorest performance, i.e. with the lowest voltage at high current density determines the maximum power output of the stack. The influence of this cell on the overall characteristic of the fuel cell stack is not significant as its power contribution is low. However, as was discussed in Section 4, care has to be taken that no cell reaches negative voltage. Naturally, the cells with poor performance are the first to reach this critical point. In order to allow for a proper margin of safety in practical applications, none of the cells should be operated below a threshold level of 0.5–0.6 V.

With a suitable diagnosis system, the fuel cell current is limited to the value, where the first cell reaches the lower boundary voltage, even when all other cells would permit an increase in current. The maximum power output of the fuel cell stack also settles at this current level. As the voltage is not only dependent on the current, but also on many other parameters, such as temperature, humidity, and pressure, the operating range of the fuel cell cannot be correlated a priori to a particular current range, i.e., at low temperatures the boundary voltage is reached at a lower current level than at higher temperatures. Therefore, the maximum current needs to be regulated by a “watchdog” monitoring the single-cell voltages.

5.2. Pressure drop

Fig. 5 shows the measured pressure drop across the stack. The pressure drop appears to increase linearly with the mass flow. But, the data was fitted by a parabolic equation since it produced better results. On the one hand, this relationship between pressure drop and flow-rate seems to justify the assumption of a laminar flow in the fuel cell flow field. Flow friction caused by hydraulic resistances (such as sharp edges, discharge into the manifold from the narrow channels), which typically increase quadratic with the flow rate, seem to have only a small effect but explain the slight parabolic tendency observed in the measurement. However, on the other hand, the flow resistance of bends is found to increase considerably for laminar flows with Reynolds number, $Re < 100$ [9]. And if this increase is assumed to be proportional to the inverse Reynolds number, a linear pressure drop, flow-rate relationship is obtained. Furthermore, very few studies have been devoted to two phase flows in

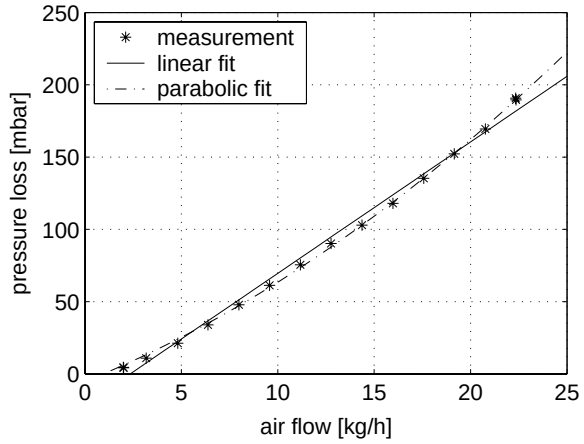

Fig. 5. Measured pressure drop of the cathode side in 100-cell stack. Stack was operated at 30 A (0.15 A/cm^2) for 30 min prior to recording. Cell temperature, 60 °C; air dew point, 45 °C; air stoichiometry, 2.2; air/hydrogen pressure, 2/2.2 bar_{abs}.

manifolds and bends, especially at very low Reynolds numbers. Therefore, any conclusion drawn from the observed relationship between pressure drop and flow rate needs to be treated with caution.

Using the Hagen–Poiseuille equation for laminar flows the flow friction is calculated as follows:

$$f = \frac{64}{Re} \quad \text{with} \quad Re < 2300 \tag{4}$$

Assuming a single phase flow the pressure drop is then determined by Eq. (5):

$$\Delta p = \frac{v32\eta l}{d^2} \tag{5}$$

where v is the mean flow velocity, η the viscosity, l the channel length and d the hydraulic diameter.

The presence of water droplets suggests the existence of a two-phase flow in the channels. The pressure drop for a two-phase flow is then calculated by applying the trapezoidal rule on Eq. (6) [10].

$$\Delta p = \int_0^l \left[G^2(y) \left(\frac{2(yf(y) + K)\upsilon_g(y)}{d} \times \left(1 + \frac{x(y)\upsilon_{fg}(y)}{2\upsilon_g(y)} \right) \right) \mathrm{d}y \right] \tag{6}$$

where G is the mass velocity, y the axial co-ordinate, υ_g the specific volume of the gas phase, υ_{fg} the difference in specific volume between the gas and liquid phases and x the mass vapor quality.

The estimated pressure drops for a single-phase flow and a two-phase flow using the original channel dimensions and disregarding the effect of the bends are both shown in Fig. 6. Not surprisingly, large deviations are observed between model predictions of the pressure drop and measurement data. The calculated values amount to only 10% of the measured values. One possible explanation for the large

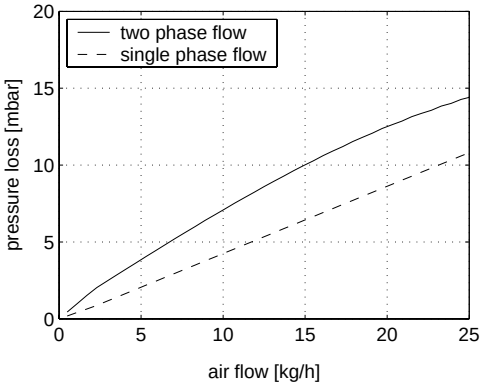

Fig. 6. Simulated pressure drop for single and two phase flow on the cathode side in 100-cell stack. Air pressure, 2 bar_{abs}; channel height, 0.55 mm; channel width, 0.95 mm; channel length, 0.415 m; hydraulic resistance, $K = 0$.

discrepancy between simulation and measurement is found in the compressibility of the gas diffusion electrode. Any swelling of the membrane may be neglected, since these changes are very small (∼ 5–10 μm). However, with a thickness of around 0.45 mm the gas diffusion electrodes are assumed to have an effect on the flow in the channels. Since the gas diffusion electrodes are pressed between two flow field plates (together with the membrane), they intrude into the flow channels. This intrusion translates into a decrease of the channel cross-section, thus resulting in an increase of the flow friction.

The discrepancy between the simulation and the measurement results fosters speculations about the disregard of the effect of the bends in the flow channels. The flow field has a meander structure in which each channel has eight bends. Assuming a value of 0.1 for the hydraulic resistance K for each bend and reducing the channel height slightly, a better agreement between measurement data and simulation is achieved, as shown in Fig. 7. Here, the effects of the bends

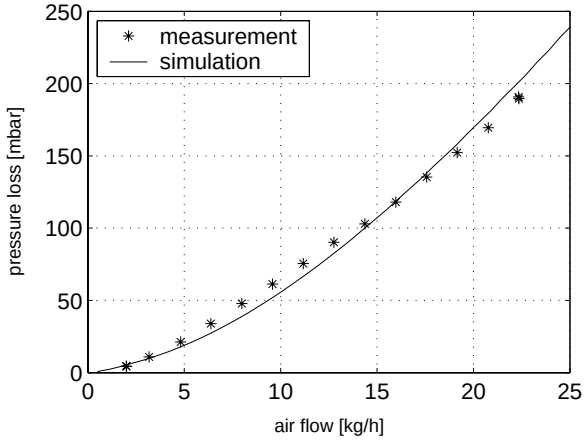

Fig. 7. Comparison of experimental values and simulated pressure drop for two phase flow on the cathode side in 100-cell stack. Air pressure, 2 bar_{abs}; channel height, 0.465 mm; channel width, 0.95 mm; channel length, 0.415 m; hydraulic resistance, $K = 0.8$.

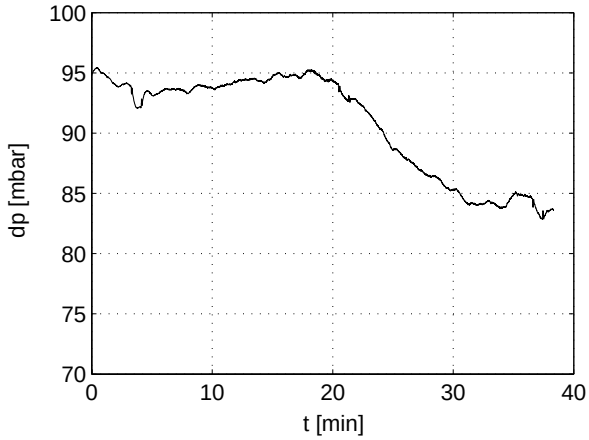

Fig. 8. Measured decrease of pressure drop across stack as the result of a reduction in current from 40 A (0.2 A/cm^2) to 20 A (0.1 A/cm^2) at $t = 20$ min. Cell temperature, 60 °C; air dew point, 45 °C; air flow, 12.8 kg/h; air/hydrogen pressure, 2/2.2 bar$_{abs}$.

outweigh the effect of the reduced channel height by far. Hence, by disregarding the effects of bends, the flow in the channels is not correctly represented. Nevertheless, is was found that the pressure loss scales almost linearly with the mass flow. Thus, for control purposes it is adequately represented by an empirical equation.

Additionally, water in the flow channels affects the pressure loss in the flow channels. In the course of the experiment shown in Fig. 8, the air mass flow rate was kept unchanged and the relative humidity at the inlet was set 35 ± 5%. However, the current was reduced by 50% at $t = 20$ min from 40 A (0.2 A/cm^2) to 20 A (0.1 A/cm^2), thus applying dry conditions to the fuel cell stack in the second half of the experiment. Once the current is reduced, the pressure drop decreases slowly and after about 10 min settles to a new value, which is about 10% lower than the previous pressure drop. The reduction of the current reduces the flux of product water in the flow channels, and therefore reduces the total mass flow in the flow channels. Therefore, a decrease of the pressure drop is also predicted by the simulation, though this decrease is instantaneous. The large time constant observed in the experiment suggests that water is gradually removed from the MEA. The water droplets are then driven out of the channels, hence the channel cross-section is enlarged and the flow resistance is reduced.

6. Performance improvements

In this section procedures are described which have a beneficial effect on the fuel cell stack performance. These procedures are simple to realize and only require minor adjustments to the control software or, in case of the flow pulsing, slight modifications of the hardware. While the power consumption of the additional devices is almost negligible, the improvements they permit in efficiency and long-term stability are considerable.

6.1. Current pulsing

Performance decrease of cells operating at low current densities has been suggested to result from changes of the Pt catalyst particle surface. Partial oxide coverage of the active Pt surface reduces the rate of the oxygen reduction reaction at the cathode [11]. Short excursions to high current densities (or low voltages) showed improvements in performance due to the removal of oxygenated species from the Pt surface. In [12] a method is described by which a fuel cell is periodically starved at the anode. These momentary fuel starvation conditions are believed to cause the anode potential to increase, resulting in the oxidation and removal of poisons from the anode catalyst surface and an improved cell performance.

The beneficial effect of current pulses was confirmed for a large-scale fuel cell stack. Fig. 9 shows the polarization curves recorded after the fuel cell was constantly operated at 15 A for 30 min with (a) no pulses and (b) with pulses of 35 A and a duration of 2 s at a duty rate of 3.33%. Due to the specific test procedure in which the current is increased in steps from 0 to 70 A and again reduced back to 0 A, two sets of measurement points are obtained. The respective sets are fitted with the following equation:

$$E = E_0 - b \log i - Ri$$
$$E_0 = E_r + b \log i_0 \quad (7)$$

where E is the cell voltage, b and i_0 are the Tafel slope and the exchange current density, respectively, i is the current density, R is the ohmic resistance, and E_r is the reversible potential.

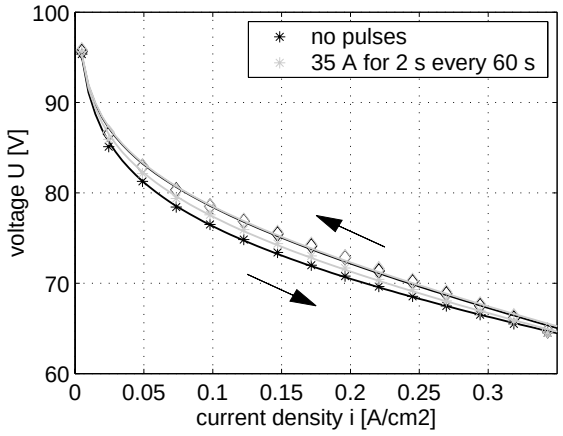

Fig. 9. Measured polarization curves recorded after the stack was operated at 15 A for 30 min (0.075 A/cm^2). Cell temperature, 60 °C; air dew point, 45 °C; air stoichiometry, 2.2; air/hydrogen pressure, 2/2.2 bar$_{abs}$. At each measurement point the current was held for 20 s and the voltage allowed to settle down. The upward slope (0 to 70 A) is represented by the star symbol and the downward slope (70 to 0 A) by the diamond symbol.

The hysteresis observed in Fig. 9 between upward and downward slopes may result either from the formation of Pt oxides at high cathode potentials, from the build-up of impurities on the catalytic surface, from partial dehydration of the catalyst layer due to limited water generation at high cathode potentials or from a combined effect. By applying current pulses to the fuel cell, the voltage in the upward slope (when the current is changed from 0 to 70 A) was increased, especially in the low to medium current density range. The fitted Tafel slope coefficient b in the low current density region ($E > 0.75$ V) is 59 mV/dec for the upward slope of case (a) with no pulses and 56 mV/dec for the upward slope of case (b) with pulses. This change indicates that current pulses improve the oxygen reduction reaction rate. For the downward slope a fitted value for b of 53 ± 0.5 mV/dec is obtained in the low current density region for both cases, indicating that similar kinetic conditions exist in both cases. Hence no difference in voltage is observed in the downward slopes.

The effect of enhanced water generation due to the current pulses is considered beneficial although small, since the duration of the current pulses is short (2 s every 60 s). The fine reproducibility of the difference in voltage between the experiments with pulses and without pulses is not in line with the effect of impurities on the oxygen reduction reaction rate. These are expected to be of stochastic nature. Thus, the formation of Pt Oxides most likely explains the change. Under steady-state conditions the coverage with oxygen-containing species is found to increase approximately linearly with the potential [13], and the build-up of this Pt oxide layer is effectively impeded by short excursions to lower potentials. Therefore, no difference is observed in the voltage of the downward slope, since most oxygen-containing species are removed in the low-voltage regions and the renewed build-up is equal for both cases.

6.2. Flow and pressure pulsing

Previous experiments [5] had revealed the beneficial effect of pressure pulses in the supply system, especially on the hydrogen side (Fig. 10). With the setup described in Section 3 shock waves are generated which move at great speed through the flow channels, thereby dispersing water droplets that may have formed inside. The wave is followed by a temporary increase in flow, which blows the water particles out of the stack.

Furthermore, the diffusion layer between the flow channel and the membrane is assumed to be dynamically inflected by the pressure wave [14]. These recurring expansions and contractions support the removal of unwanted liquid fluid from the diffusion layer and the supply of hydrogen to the same.

6.3. Differential pressure

The water flux due to back-diffusion is roughly inversely proportional to the membrane thickness, whereas the flux

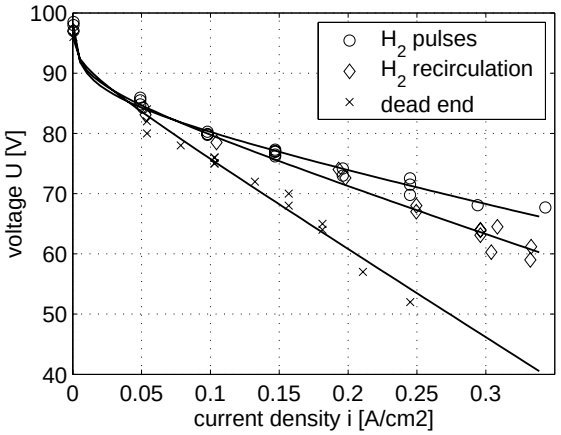

Fig. 10. Measurements showing the advantage of a pulsed hydrogen supply over a system where excess hydrogen is recirculated by means of a pump. Cell temperature, 60 °C; air dew point, 45 °C; air stoichiometry, 2.2; air/hydrogen pressure, 2/2.0 bar_{abs}. At each measurement point the current was held for 20 s and the voltage allowed to settle down.

due to the electro-osmotic drag is independent of the thickness [15,16]. When thin membranes such as Nafion 112 are used, back-diffusion can effectively compensate the effects of the drag. Thus liquid water accumulated in the cathode is drawn by a concentration gradient across the membrane to the anode and removed with the excess hydrogen stream [17]. However, the flux due to back-diffusion might overcompensate the flux due to the electro-osmotic drag, leading to the accumulation of liquid water in the anode. Since the hydrogen flow is small these water droplets are difficult to remove from the anode, especially at low current densities. If the hydrogen pressure is set slightly higher (0.2 bar) than the air pressure, an additional force is applied on the water molecules in the membrane, which drives liquid water towards the cathode and prevents accumulation in the anode.

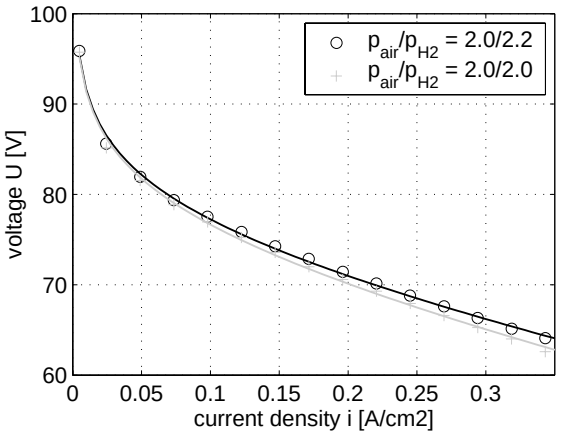

Fig. 11. Measurements showing the beneficial effect of a differential pressure across membrane. Prior to measurement the fuel cell was exposed to wet conditions (air dew point > stack temperature) for several hours. Cell temperature, 40 °C; air dew point, 45 °C; air stoichiometry, 2.2. At each measurement point the current was held for 20 s and the voltage allowed to settle down.

Fig. 11 shows the beneficial effect of a slight pressure difference across the membrane. Prior to the recording of these polarization curves, the fuel cell was operated for several hours under wet conditions (i.e., the air dew point was higher than the stack temperature). Furthermore, data on the amount of water collected in the water trap at the anode exit qualitatively confirmed the assumption that more water is removed with the fuel stream when no pressure difference is applied. If the fuel cell is operated under dry conditions (i.e., the air dew point is lower than the stack temperature) no increase in voltage is observed with a higher anode pressure.

7. Conclusion

Measurements from a testbench with a 6 kW, 100-cell PEM stack were used to investigate some aspects critical to the operation of large fuel cell stacks in automotive applications. First, typical failures such as negative voltage due to reactant undersupply, leaks in the membrane due to hot spots, as well as large differential pressure were outlined. The importance of monitoring individual cell voltage was stressed, since the cell with the lowest voltage in the stack restricts the maximum power output of the stack. Second, the cause for variations in the cell voltages across the stack was discussed. Typically these are a cumulative result of uneven flow distributions of the reactant gases, a non-uniform temperature field, ageing and manufacturing defects. Finally, several procedures were proposed which have a beneficial effect on the fuel cell performance. Current pulsing proved to be very effective in impeding the build up of a Pt oxide layer and the related decrease in performance. Flow and pressure pulsing as well as a differential pressure across the membrane facilitate the removal of liquid water from the flow channels.

References

[1] A. Parthasarathy, S. Srinivasan, A.J. Appleby, C.R. Martin, J. Electrochem. Soc. 139 (1992) 2856.
[2] M.R. Tarasevich, A. Sadkowski, E. Yeager, Kinetics and Mechanisms of Electrode Processes, in: B.E. Conway, J. O'M. Bockris, E. Yeager, S.U. Khan, R.E. White (Eds.), Comprehensive Treatise of Electrochemistry, Vol. 7, Plenum Press, 1980.
[3] P. Rodatz, O. Garcia, L. Guzzella, F. Büchi, M. Bärtschi, A. Tsukada, P. Dietrich, R. Kötz, G. Scherer, A. Wokaun, SAE Technical Paper 2003-01-0418 in: Proceedings of the SAE World Congress, 2003.
[4] M. Ruge, F.N. Büchi, in: Proceedings of the First European PEFC Forum, Lucerne, 2–6 July 2001.
[5] P. Rodatz, A. Tsukada, M. Mladek, L. Guzzella, in: Proceedings of IFAC 15th World Congress, Barcelona, Spain, 21–26th July 2002.
[6] M.H. Fronk, D.L. Wetter, D.A. Masten, A. Bosco, SAE Technical Paper 2000-01-0373.
[7] M. Wöhr, K. Bolwin, W. Schnurnberger, M. Fischer, W. Neubrand, G. Eigenberger, Int. J. Hydrogen Energy 23 (1998) 213.
[8] J. St-Pierre, D.P. Wilkinson, S. Knights, M.L. Bos, J. New Mater. Electrochem. Syst. 3 (2000) 99.
[9] W. Wagner, Vogel Fachbuch, Kamprath-Reihe, 2001.
[10] P. Argyropoulos, K. Scott, W.M. Taama, Chem. Eng. J. 73 (1999) 217.
[11] F.A. Uribe, T.A. Zawodzinski, Electrochim. Acta 47 (2002) 3799.
[12] D.P. Wilkinson, C.Y. Chow, D.E. Allan, E.P. Johannes, J.A. Roberts, J. St-Pierre, C.J. Longley, J.K. Chan, US Patent 6,096,448 (2000).
[13] A. Damjanovic, V. Brusic, Electrochim. Acta 12 (1967) 615.
[14] C.M. Carlstorm, W.B. Maynard, US Patent 6,093,502 (2000).
[15] T.E. Springer, T.A. Zawodzinski, S. Gottesfeld, in: Proceedings of the Symposium on Modeling of Batteries and Fuel Cells, vol. viii+403, Electrochemical Society, Pennington, NJ, USA, 1991, pp. 209–229.
[16] F.N. Büchi, G.G. Scherer, J. Electrochem. Soc. 148 (2001) A183.
[17] D.P. Wilkinson, H.H. Voss, K. Prater, J. Power Sources 49 (1994) 117.